Journal of Materials Chemistry

www.rsc.org/materials

Volume 19 | Number 9 | 7 March 2009 | Pages 1193–1340

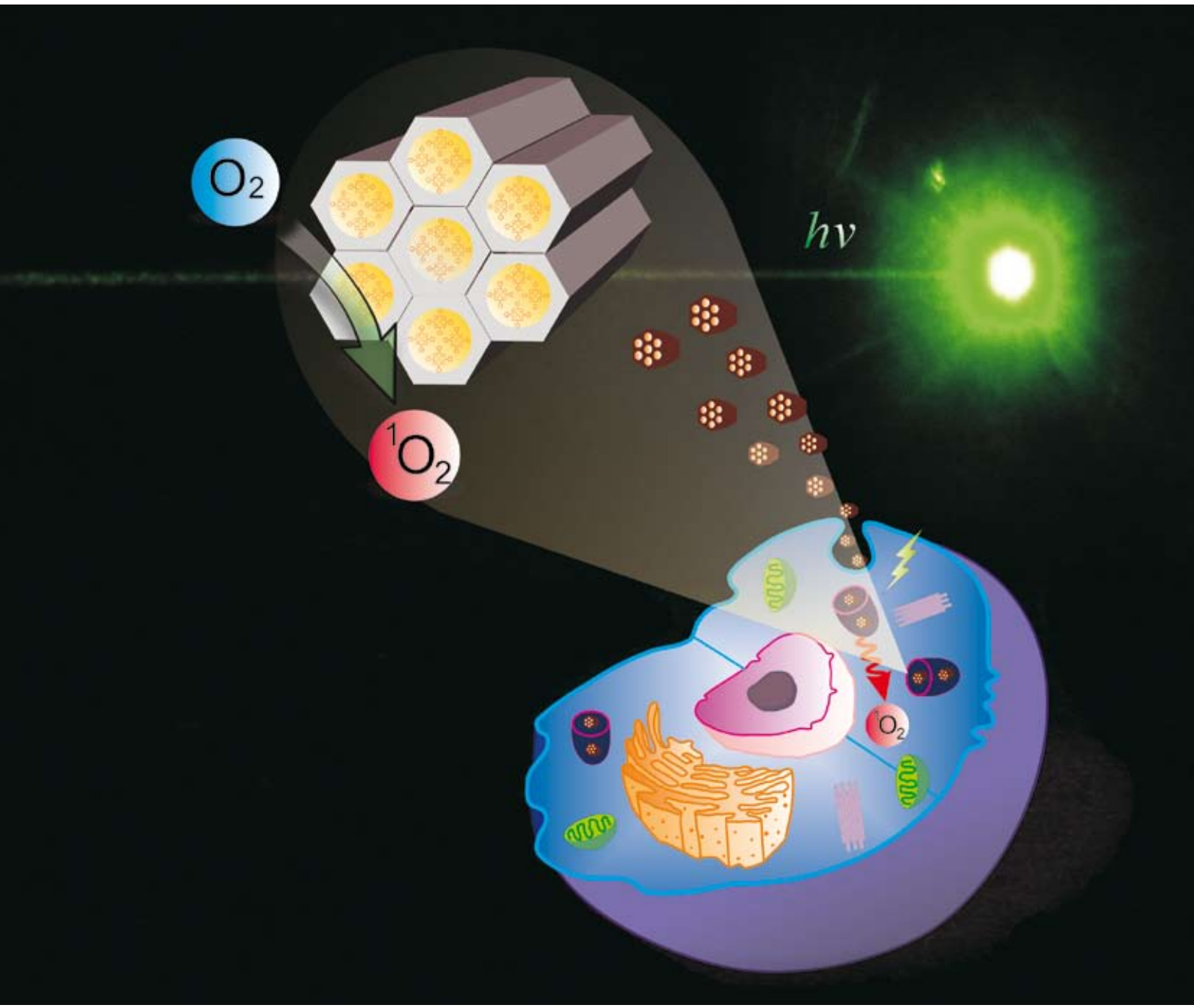

ISSN 0959-9428

RSC Publishing

Mesoporous silica nanoparticles functionalized with an oxygen-sensing probe for cell photodynamic therapy: potential cancer theranostics

Shih-Hsun Cheng,[ac] Chia-Hung Lee,[b] Chung-Shi Yang,[b] Fan-Gang Tseng,[c] Chung-Yuan Mou[d] and Leu-Wei Lo*[a]

Received 24th September 2008, Accepted 19th November 2008
First published as an Advance Article on the web 8th January 2009
DOI: 10.1039/b816636f

Functionalization of mesoporous silica nanoparticles (MSNs) with Pd-porphyrins for cancer cell photodynamic therapy is reported. The composite platform, MSN–PdTPP, expands the role of Pd-porphyrins from their routine use as phosphorescence probes for oxygen sensing/imaging (diagnostics) to that of novel nano-photosensitizers for cancer cell phototherapy (therapeutics). The utility of MSN–PdTPP in the phototherapeutic treatment of MDA-MB-231 breast cancer cells is also evaluated, suggesting it is a promising cancer theranostic platform.

Introduction

Theranostics, a term that reflects the dual therapeutic and diagnostic utility of a compound or methodology, has emerged as an important concept in the contemporary design of nanotechnology-based molecular imaging contrast agents and imaging-guided therapeutics.[1,2] In particular, the enhanced permeability of tumor vasculature and the identification of novel cancer markers that facilitate retention of i.v.-administered nanoparticles within a tumor[3] has led to the recent development of a wide range of nano contrast agents and therapeutics that include gold nanoparticles,[4] liposomes,[5–7] polymeric nanoparticles,[8–11] and mesoporous silica materials.[12–28] Among them, Ohulchanskyy *et al.* reported the synthesis of a novel nanoformulation of organically modified silica (ORMOSIL) nanoparticles with a covalently incorporated photosensitizer (PS), HPPH [2-devinyl-2-(1-hexyloxyethyl)pyropheophorbide], for cancer photodynamic therapy (PDT).[29] Zhang *et. al.* also developed efficient photosensitizers that exploit infrared excitation, based on photon upconverting nanoparticles (PUNPs) coated with silica matrix.[30,31]

In contrast to ORMOSIL nanoparticles and PUNPs, the silica nanoparticles we describe in this paper are comprised of mesoporous silica (termed mesoporous silica nanoparticles or MSNs) that serve as a matrix in which high densities of transportable molecules reside, shielded from their local environment. The MSNs are comprised of highly-ordered, hexagonal pores with mean particle diameters of 70–100 nm, and possess a number of unique properties that include large surface areas ($\sim$1000 m^2 g^{-1}), uniform pore diameters ($\sim$3.0 nm), ease of chemical modification, avid uptake by cells,[14,22] payload (*e.g.*, fluorophores, drugs) protection and low cytotoxicity.[19,32] Not surprisingly, MSNs have been functionalized for use in chemical catalysis,[33,34] drug delivery,[13,14,21,23–25] cell labeling,[12,17,18] and controlled release of therapeutics.[14,15]

These same properties make MSNs attractive for PDT applications as well. In particular, the MSNs' large surface areas permit conveyance of significant numbers of PSs per particle while the avid cellular uptake of MSNs enables substantial intracellular accumulation of PS for optimal PDT efficiency.

In the current study, we covalently conjugate the PS Pd-porphyrin onto the surface of MSNs and evaluate their PDT potential in the treatment of breast cancer cells. Pd-porphyrin is a synthetic metallo-porphyrin with long phosphorescence lifetime and is well known in use for quantitative *in vivo* oxygen sensing and imaging.[35–40] As described below with its conjugation to MSNs, we extend the functionality of Pd-porphyrins from their original "diagnostics" role in oxygen sensing and imaging to "therapeutics" in PDT.

PDT is based on PSs generating singlet oxygen ($^1O_2$), and subsequently reactive oxygen species (ROS) upon localized exposure to light in the presence of ground state oxygen (O_2).[41–44] After excitation of the PS from its ground singlet state to an excited singlet state, the PS undergoes intersystem crossing to a longer-lived excited triplet state. Energy transfer from the PS's excited triplet state to a nearby oxygen molecule (which posses a ground triplet state) results in the relaxation of the PS to its ground singlet state and the formation of an exicted singlet state oxygen molecule. The intrinsic cytotoxity of singlet oxygen leads to selective and irreversible destruction of diseased tissues in the vicinity of $^1O_2$. For PDT to be successful, three criteria must be met. First, to minimize systemic toxicity, the PS should be highly targeted. Second, adequate oxygen permeability/perfusion in the region of disease is critical, it directly correlates to oxidative damage to neighboring cells.[45] And finally, the adequate local

[a]*Division of Medical Engineering Research, National Health Research Institutes, 35 Keyan Road, Zhunan 350, Taiwan, ROC. E-mail: lwlo@nhri.org.tw; Fax: (+886)37-586440*
[b]*Center for Nanomedicine Research, National Health Research Institutes, 35 Keyan Road, Zhunan 350, Taiwan, ROC*
[c]*Institute of NanoEngineering and MicroSystems, National Tsing Hua University, Hsinchu 300, Taiwan, ROC*
[d]*Department of Chemistry National Taiwan University, Taipei 106, Taiwan, ROC*

concentration of PS in diseased tissue and quantum yield of singlet oxygen are needed to minimize colateral thermal damage from photoirradiation.

Porphyrin derivatives without chelating metal ions are conventional PSs for PDT: both *in vitro* and *in vivo*.[46–48] For our studies, however, we use a phosphorescent Pd-meso-tetra(4-carboxyphenyl) porphyrin (PdTPP) as the PS. As noted earlier, PdTPP is a metallo-porphyrin that is frequently used to measure oxygen distributions in tissues *via* oxygen-dependent quenching of phosphorescence.[36,37] The long-lived triplet state of PdTPP is produced with unity quantum yield, while the concentration of singlet oxygen generated in PDT depends on the accessibility of the excited PdTPP to oxygen.

The energy of photoirradiation required in phosphorescence imaging is generally only 10^{-4}–10^{-5} times that typically used in PDT.[36,49] Consequently, the concentration of singlet oxygen generated *via* PdTPP during oxygen sensing/imaging from phosphorescence quenching is much less than that generated during PDT. Thus PdTPP, as currently used in oxygen sensing/imaging, has negligible therapeutic benefit. But by simply changing the energy of photoirradiation, PdTPP can be made to switch between being a phosphorescence probe for oxygen sensing/imaging (diagnostics)[24–26] and a PS for PDT (therapeutics).

To achieve high PDT efficacy, the ability of PS to enter cells is critical, since the short-lived singlet oxygen can then directly interact with intracellular machinery for maximal cytotoxicity. High cellular uptake of MSNs by endocytosis has been previously reported.[15–20] We thus elected to use MSNs as nanocarriers of PdTPP, to enter the intracellular milieu for subsequent photoirradiation. Due to the enormous porosity and surface area of MSNs, PdTPP can readily be covalently bonded to MSNs and remain well-protected from its local environment, within a rigid porous structure. Generation of singlet oxygen arises from energy transfer to the molecular ground state oxygen as it diffuses through the pore matrix, which is simply connected (topologically) to the exterior of the MSN. Shielding of the PS afforded by the MSN also obviates the degradation of PS and its release into systemic circulation.[29,50] The enormous surface area of MSNs permits efficient delivery of high concentrations of PdTPP, thereby decreasing the energy of photoirradiation needed to achieve the efficient oxidative cytotoxicity.

Experimental

Synthesis of MSNs

The MSNs were synthesized under low concentration tetraethoxysilane (TEOS, Acros) surfactant and a base catalyst (NH_4OH), in a two-step preparation.[51] The sol–gel process for the co-condensation of TEOS and 3-Aminopropyl-trimehoxy silane (APTMS, Acros), to synthesize MSNs-APTS intermediate was as follows. First, 0.1 g of CTAB was dissolved in 50 g of 0.51 M NH_4OH at 50 °C, and 0.8 mL of 0.2 M dilute TEOS (in ethanol) was added with vigorous stirring. After the solution had been stirred for 5 h, 0.8 mL of 12% (v/v) APTMS (in ethanol) and 0.8 mL of 1.0 M TEOS were added, followed by vigorous stirring for another 1 h. The solution was then aged at 50 °C for 24 h. Solid samples were collected *via* centrifuging at 12 000 rpm for 20 min, washing, and redispersing with deionized water and ethanol several times. Surfactant templates were removed by extraction in acidic ethanol (0.17 g of HCl in 9 mL of ethanol at 65 °C for 24 h).

Preparation of MSNs-PdTPP

First, we dissolved Pd-meso-tetra (4-carboxyphenyl) porphyrin (20mg, 0.022 mmole) in methanol (30 mL). We then added APTMS solution (2 ml, 95%) and *N*-Ethyl-*N*′-(3-dimethylaminopropyl)carbodiimide hydrochloride (EDC, 69.2 mg, 0.445 mmole) into the solution and stirred the mixture gently for 24 h at room temperature. 3 ml of the resulting reaction mixture was then added to 50 ml of the MSN solution (11 mg ml^{-1}, 30 ml) and stirred at 60 °C for 12 h. The MSN–PdTPP complex was then washed with methanol and PBS solution twice; and centrifuged at 12 000 rpm for 17 min. The degree of PdTPP loading in MSNs was determined by measuring the optical absorbance at 400 nm (Soret Band of PdTPP) as the MSN matrix was dissolved with HF-NaF2; yielding a maximal loading of 2.3 wt% PdTPP with respect to MSNs.

Characterization

Steady-state spectra were acquired with a DU800 UV spectrometer (Beckman) and Cary Eclipse Fluorescence spectrometer (Varian). FT-IR spectra were recorded on a Jasco FT/IR 4200 spectrometer using a KBr pellet. Approximately 1 mg of MSN–PdTPP was mixed with 300 mg of dried KBr and then compressed. Surface area and pore size were determined by N_2 adsorption–desorption isotherm measurements at 77 K on a Micrometric ASAP 2010 volumetric adsorption analyzer once the sample had been outgassed at 10^{-3} Torr and 120 °C for 6 h. Pore size distribution curves were obtained from Barrett–Joyner–Halenda (BJH) analysis of the desorption isotherms while MSN morphology was characterized with transmission electron microscopy (Hitachi H-7650 TEM) operating at 80 kV.

Cell culture

MDA-MB-231 cells, a human caucasian breast adenocarcinoma cell line, was kindly provided by Dr. Kurt M. Lin at the Division of Medical Engineering Research, National Health Research Institutes, Taiwan and grown in conventional growth medium consisting of RPMI-1640 (GIBCO) with 10% fetal bovine serum (FBS) (GIBCO), 100 U/ml penicillin, and 100 μg ml^{-1} streptomycin. All culture were maintained in 5% CO_2, 95% air, and at 37 °C.

Cell uptake and TEM imaging of nanoparticles

To determine cellular uptake of nanoparticles, MDA-MB-231 cells were first plated in 35 mm dishes containing RPMI-1640 media and 10% FBS at a density 1×10^5 cells/well. The dishes were then placed overnight in the incubator at 37 °C and 5% CO_2 to permit cell attachment. The next day, the cells were carefully washed with phosphate-buffered saline (PBS) and refreshed with 1 mL of the serum-free medium. At the same time, 50 μg MSN–PdTPP in 1 mL ethanol was centrifuged at 12 000 rpm for 17 min, followed by supernatant replacement with serum-free

medium. After 3 cycles of vortexing and centrifuging the MSN–PdTPP in serum-free medium, the washed nanoparticles were added to each well and mixed gently at a final concentration of 50 μg ml^{-1}. The treated cells were then incubated at 37 °C and 5% CO_2 for 2 h. After incubation the cells were rinsed with PBS three times.

For cell ultrasection, the treated cells were prefixed in 2.5% glutaraldehyde for 1 h and then washed twice with 0.1 M PBS (pH 7.0). 2% osmium tetroxide was used for 1 h for post-fixation. Dehydration was then performed in an ascending series of ethanol concentrations; beginning with 50%, 70%, 80%, 95% ethanol dehydrations, at 10 min each, and followed by three 100% ethanol dehydrations for 10 min each. Dehydrated samples were then embedded in Spurr resin and allowed to polymerize for 15 h at 68 °C. Ultrathin sections were cut with a Leica UC6 ultramicrotome and examined with a Hitachi H-7650 transmission electron microscope (TEM) at 80 kV accelerating voltage without further staining.

Detection of singlet oxygen

Detection of the generation of singlet oxygen ($^1O_2$) by its phosphorescence emission at 1270 nm has been extensively reported.[45] To extend the phosphorescence lifetime of $^1O_2$ in an aqueous environment, we dispersed 11.33 mg MSN–PdTPP in deuterium oxide (D_2O). 1×10^{-4}M of Rose Bengal (Aldrich) in D_2O was used as positive control. For measurement of singlet oxygen phosphorescence spectra, a TRIAX 180 spectrometer (Jobin Yvon) equipped with a high performance InGaAs photodiode (Electro-Optical Systems Inc.) was used. The light source consisted of a 532 nm diode-laser (40 ± 5 mW cm^{-2}), whose output was passed through an optical chopper (AST Instruments Corp.) operating at fixed frequency. Samples were loaded into quartz cuvettes and placed within a light-tight chamber, with the emission signal collected orthogonal to the excitation beam *via* a lock-in amplifier (Model SR530, Stanford Research Systems). An additional long-pass filter (800 cut-on) was used to attenuate higher order excitations of the laser and PdTPP phosphorescence.

We also used 1,3-diphenylisobenzofuran (DPBF, Aldrich) to determine the release of singlet oxygen into solution.[52] The reaction was monitored by recording the decrease in absorption at 400 nm *via* UV-Vis spectroscopy (DU800, Beckman). In our experiment, 50 μL of stock solution of DPBF (8 mM) was added into 3 mL of 50 μg mL^{-1} MSN–PdTPP solution in D_2O, while the control used DPBF only in D_2O and MSNs with DPBF in D_2O. Solutions were then illuminated with a 532 nm laser and the optical densities at 400 nm recorded every 5 s.

Cell phototherapy studies

For cell phototherapy studies, MDA-MB-231 cells were plated in 96-well plates at a density of 1×10^4 cells/well in RPMI-1640 media with 10% FBS, and incubated overnight at 37 °C and 5% CO_2. The next day, cells were carefully rinsed with PBS and replenished with 100 μL/well of serum-free medium. At the same time MSN–PdTPP preparations of 50 μg, 25 μg, 10 μg in 1 mL ethanol were centrifuged at 12 000 rpm for 17 min, followed by supernatant replacement with serum-free medium. MSN–PdTPP was washed with ethanol, and then the ethanol was replaced with serum-free medium. The MSNs–PdTPP specimens were then washed with medium three times and administered to cells at final concentrations of 50 μg ml^{-1}, 25 μg ml^{-1}, 10 μg ml^{-1} per well. Following 2 h of incubation at 37 °C and 5% CO_2, plates were immediately exposed to a 532 nm laser operating at 40 ± 5 mW cm^{-2} for doses of 1.2 J, 2.4 J, 3.6 J per well. Following irradiation, wells were washed with PBS and cell viability was estimated by WST-1 assay, propidium iodide (PI) stain and changes of cell morphology. In the WST-1 assay, tetrazolium salt WST-1{4-[3-(4-Iodophenyl)-2-(4-nitrophenyl)-2H-5-tetrazolio]-1,3-benzene disulfonate} in live cells was cleaved by mitochondrial dehydrogenase activity to yield formazan. After 532 nm irradiation, cells were removed and placed into 100 μl/well serum-free medium and 10 μl/well Cell Proliferation Reagent WST-1 (Roche). The plates were then incubated for 4 h. After incubation with WST-1, plates were shaken for 1 min and measured for optical absorbance at 450 nm using an ELISA reader (Infinite M200, TECAN). For control experiments, cells were exposed to light without treatment with MSNs–PdTPP. Three specimens were run per MSN–PdTPP concentration and light dose, with each experiment being repeated three times.

Results and discussion

In Fig. 1a we show a schematic representation of our theranostic nano-platform MSN–PdTPP. The MSNs were labeled with PdTPP *via* covalent bonding (Fig. 1b). To verify that the conjugation of PdTPP to MSN was not merely a physical association, silica-gel thin layer chromatography (TLC) of PdTPP, MSN–PdTPP, and the supernatant of MSN–PdTPP in methanol were performed (Fig. 2a). As shown in Fig. 2a, the MSN–PdTPP did not migrate with the organic solvent (lane 2); on the contrary, the PdTPP was in the front of the direction of solvent (lane 1). Furthermore, no signal whatsoever appeared in the MSNs–PdTPP supernatant lane of the plate (lane 3). The absence of PdTPP leached by organic solvent in the TLC studies indicates stable conjugation of PdTPP to MSNs.

In addition to TLC, FTIR was used to evaluate the covalent bonding of MSN and PdTPP. Two strong absorption bands were observed in the spectra (Fig. 2b), with amide I (1650 cm^{-1}, carbonyl stretch) and amide II (1540 cm^{-1}, CN stretch and NH bend) evident.[53] The FTIR spectra provide strong support for the

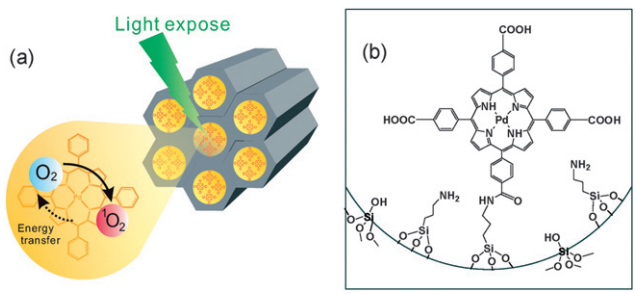

Fig. 1 (a) A photodynamic model of mesoporous silica nanoparticles (MSNs) and (b) the covalent modification of PdTPP onto the nano-channel surface of MSNs.

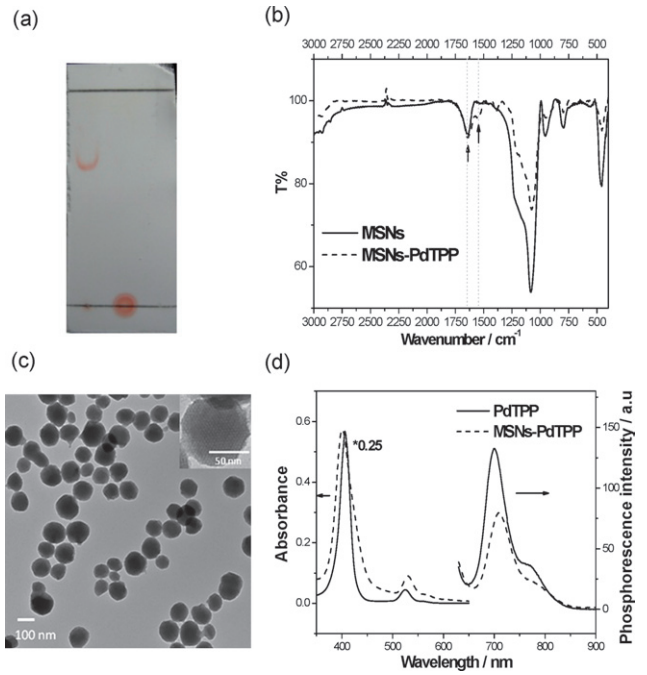

Fig. 2 (a) TLC chromatograms of PdTPP (lane 1), MSN–PdTPP (lane 2) and the supernatant of MSN–PdTPP (lane 3). (b) The FTIR spectra shows the characteristic peak of amide bond which was self-assembled with PdTPP and MSNs. The peaks of amide I (1650 cm^{-1}, carbonyl stretch) and amide II (1540 cm^{-1} CN stretch and NH bend) were observed (arrow). Both MSNs modified with (dash lane) and without (solid lane) PdTPP were shown in the spectra. (c) A TEM image of MSN–PdTPP. (d) The absorption and phosphorescence spectra of PdTPP bound to 2% albumin in PBS (solid lane) and MSNs–PdTPP dispersed in ethanol (dashed lane). The absorption of MSNs–PdTPP was 0.25 fold to that of PdTPP. The excitation wavelength was 532 nm for both PdTPP and MSN–PdTPP.

assertion that PdTPP attachment to MSNs was by means of amide bonds.

Transmission electron microscopy (TEM) revealed uniform tertiary structure of MSN–PdTPP, with an average particle diameter of approximately 100 nm (Fig. 2c), while N_2 adsorption–desorption isotherm measurements provided surface area and pore size data. After PdTPP modification, the surface area and mean pore diameter of MSNs decreased from 1026 $m^2\ g^{-1}$ and 3 nm to 540 $m^2\ g^{-1}$ and 2.3 nm, respectively, which implied the majority of PdTPP conjugation took place within the MSN's nanochannels. In Fig. 2d, PdTPP and MSNs–PdTPP in PBS with 2% bovine serum albumin show similar absorption and phosphorescence spectra.

The PDT-induced cytotoxicity of type II PS is attributed to the generation of singlet oxygen.[54] We observed singlet oxygen produced following photoirradiation of MSN–PdTPP by its characteristic phosphorescence at 1275 nm, and by its reaction with 1,3-diphenylisobenzofuran (DPBF) resulting in the decrease of DPBF's absorption at 400 nm.[52] Fig. 3a displays the phosphorescence spectra of singlet oxygen generated by Rose-Bengal and MSN–PdTPP with 532 nm excitations. Instead of water, D_2O was used as the dispersion solvent to extend the phosphorescence lifetime of singlet oxygen to facilitate measurements.[55] As seen in Fig. 3a, the signature phosphorescence emission of

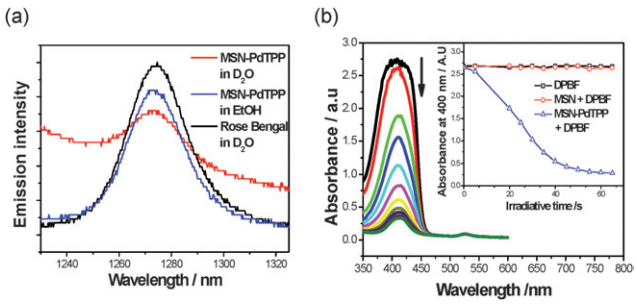

Fig. 3 (a) Phosphorescence emission of singlet oxygen generated by photoirradiation of MSNs–PdTPP dispersed in D_2O (red) and ethanol (blue). Rose Bengal in D_2O (black) was used as the standard for singlet oxygen phosphorescence measurement. The excitation wavelength was 532 nm with diode laser and the emission signal was amplified through lock-in amplifier. (b) Photobleaching of DPBF by singlet oxygen generated from MSN–PdTPP upon photoirradiation at 532 nm. Inset: decay curves of DPBF absorption as function of irradiative time in D_2O (□), in MSNs solution (○) and in MSNs–PdTPP solution (△).

singlet oxygen at 1275 nm was clearly observed under 532 nm excitation of dispersed MSN–PdTPP in D_2O. The singlet oxygen generated by Rose Bengal, a widely used singlet oxygen producer, was also measured as a positive control. Fig. 3b illustrates the photobleaching of DPBF in D_2O in the presence of MSN–PdTPP. The DPBF solution and non-conjugated MSN in DPBF solution were measured as control experiments. The steep decrease of DPBF absorption with time in the MSN–PdTPP solution indicates the efficient generation of $^1O_2$.

TEM images illustrates the MSN–PdTPP uptake by MDA-MB-231 cells, from the initiation of particle internalization (Fig. 4a) to the completion of endocytosis (Fig. 4b). The size of the vesicles enveloping MSN–PdTPP revealed by TEM is around 400 nm. It suggests the vesicles might be the late endosome or lysosome. The high cell uptake of MSN–PdTPP enables the short-lived singlet oxygen can then directly interact with intracellular machinery for maximal cytotoxicity.

The photo-induced cytotoxicity of MSN–PdTPP was then evaluated. The morphology of MDA-MB-231 cells without MSNs–PdTPP treatment shows no significant change under photoirradiation (Fig. 5a–b). On the contrary, for MDA-MB-231 cells treated with 25 μg MSNs–PdTPP for 2 h, violent

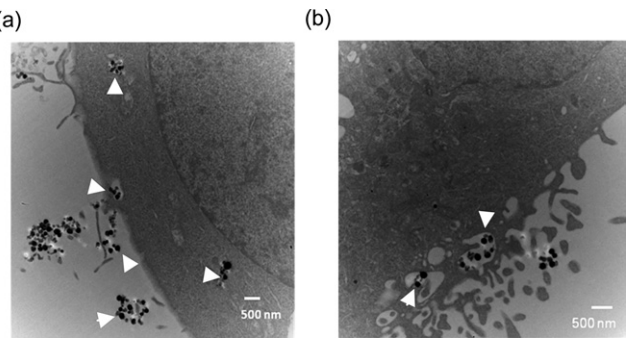

Fig. 4 TEM image of MDA-MB-231 cells treated with 50 μg ml^{-1} MSN–PdTPP for 2 h. (a) The size of nanoparticles was around 100 nm (arrow) and the cell uptake of nanoparticles was observed. (b) The vesicles containing nanoparticles were observed in the cytoplasm (arrow).

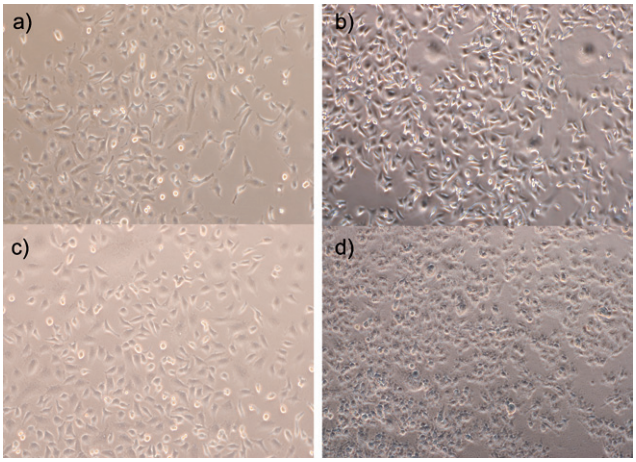

Fig. 5 The morphology of MDA-MB-231 cells treated without (the first row) and with 25 μg ml^{-1} of MSNs–PdTPP (the second row). Left column (a, c): before irradiation. Right column (b, d): 1 min after irradiation with 532 nm diode laser (total energy: 1.2J cm^{-2}).

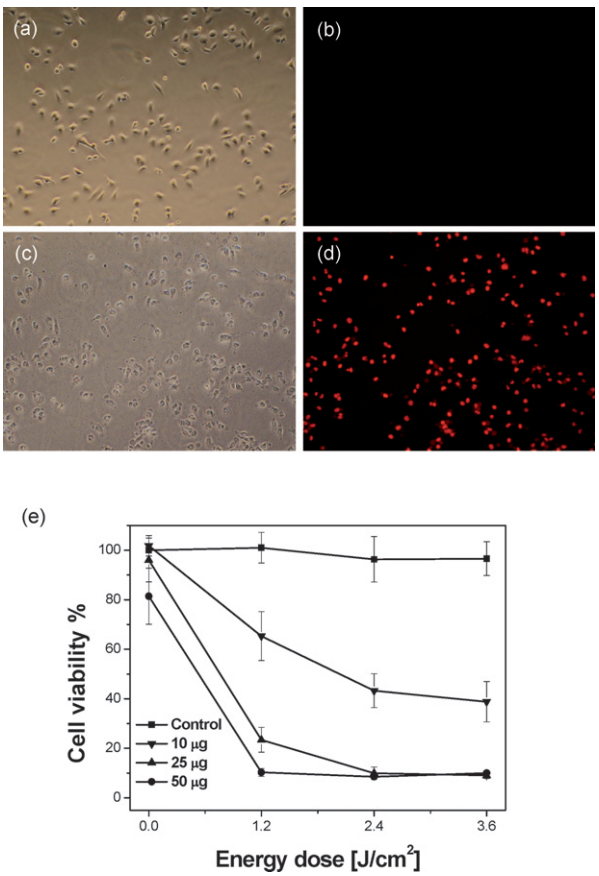

Fig. 6 Propidium iodide (PI) staining of MDA-MB-231 cells treated with 25 μg ml^{-1} of MSN–PdTPP and incubated at 37 °C for 2 h. (a) and (c) show the cell morphology, and (b) and (d) represent the PI fluorescence patterns of cells before (the first row) and after (the second row) irradiation with 532 nm diode laser for total energy of 1.2 J cm^{-2}. (e) PDT efficacy (indicative with MDA-MB-231 cell viability %) *vs.* different concentrations of MSNs–PdTPP and doses of irradiative energy with 532 nm laser. The control experiment was cells without MSN–PdTPP under the same irradiative energy.

changes in cell morphology were observed after irradiation with 532 nm laser (total energy: 1.2 J cm^{-2}) (Fig. 5c–d).

Following the PDT treatment, the propidium iodide (PI) staining of the cell was performed to evaluate the photo-induced cell death and assess its responsive pathway. The fluorescence patterns of PI staining MDA-MB-231 cells treated with 25 μg ml^{-1} of MSN–PdTPP before (Fig. 6b) and after (Fig. 6d) 532 nm laser irradiation were imaged. The prominent red fluorescence of PI was only observed in the cells after photoirradiation (Fig. 6d). It suggests that the photo-induced MDA-MB-231 cell death was mainly caused *via* necrosis. The viability of MDA-MB-231 cells treated with 10 μg ml^{-1}, 25 μg ml^{-1} and 50 μg ml^{-1} MSN–PdTPP before and after various laser irradiations were measured. In this study, three different doses of photoirradiation at 1.2 J cm^{-2}, 2.4 J cm^{-2} and 3.6 J cm^{-2} were applied. Fig. 6e indicates MSN–PdTPP concentrations less than 25 μg ml^{-1} exhibit low cytotoxicity before photoirradiation, and the optimal PDT-induced cell death could be achieved while the MSN–PdTPP concentration is higher than 25 μg ml^{-1} and the photoirradiation energy is larger than 2.4 J cm^{-2}.

Conclusions

The significant photo-induced cytotoxicity we observed in our MDA-MB-231 breast cancer studies is most likely due to a number of factors, principal of which are the high concentration of PdTPP conjugated within MSNs and the role that MSNs play as a facilitator for endocytotic cell uptake that dramatically increases the intracellular density of singlet oxygen upon photoirradiation. As such, MSN–PdTPP is a promising PS for PDT. And with the ability of PdTPP to serve as an *in vivo* contrast agent for oxygen sensing and imaging, MSN–PdTPP holds great promise as a useful nano-platform for cancer theranostics.

Acknowledgements

The study was conducted with the support of NHRI Intramural Research Grants MED-096-PP-04 and NM-096-PP-03 from National Health Research Institutes of Taiwan; and of the Grant NSC 96-2221-E-400-002 from the National Science Council of Taiwan. Special appreciation is given to Dr Sergei A. Vinogradov of the University of Pennsylvania (USA) and Dr Jeffrey S. Souris of The University of Chicago (USA) for their comments and support in this research. We also thank Ms Yu-Ching Chen for her assistance with TEM measurements.

References

1 B. Sumer and J. Gao, *Nanomed.*, 2008, **3**, 137–140.
2 J. R. McCarthy, F. A. Jaffer and R. Weissleder, *Small*, 2006, **2**, 983–987.
3 H. Maeda, *Adv. Enzyme Regul.*, 2001, **41**, 189–207.
4 G. F. Paciotti, L. Myer, D. Weinreich, D. Goia, N. Pavel, R. E. McLaughlin and L. Tamarkin, *Drug Deliv.*, 2004, **11**, 169–183.
5 S. P. Vyas and K. Khatri, *Expert Opin. Drug Deliv.*, 2007, **4**, 95–99.
6 Y. Diebold, M. Jarrin, V. Saez, E. L. Carvalho, M. Orea, M. Calonge, B. Seijo and M. J. Alonso, *Biomaterials*, 2007, **28**, 1553–1564.
7 Y. Ikehara and N. Kojima, *Curr. Opin. Mol. Ther.*, 2007, **9**, 53–61.
8 L. E. van Vlerken, Z. Duan, M. V. Seiden and M. M. Amiji, *Cancer Res.*, 2007, **67**, 4843–4850.
9 B. Schuster, *Angew. Chem., Int. Ed.*, 2007, **46**, 8744–8746.

10 X. Yuan, L. Li, A. Rathinavelu, J. Hao, M. Narasimhan, M. He, V. Heitlage, L. Tam, S. Viqar and M. Salehi, *J. Nanosci. Nanotechnol.*, 2006, **6**, 2821–2828.
11 L. E. van Vlerken and M. M. Amiji, *Expert Opin. Drug Deliv.*, 2006, **3**, 205–216.
12 S. H. Wu, Y. S. Lin, Y. Hung, Y. H. Chou, Y. H. Hsu, C. Chang and C. Y. Mou, *Chembiochem*, 2008, **9**, 53–57.
13 M. Vallet-Regi, F. Balas and D. Arcos, *Angew. Chem., Int. Ed.*, 2007, **46**, 7548–7558.
14 B. G. Trewyn, S. Giri, I. I. Slowing and V. S. Lin, *Chem. Commun.*, 2007, 3236–3245.
15 I. I. Slowing, B. G. Trewyn and V. S. Lin, *J. Am. Chem. Soc.*, 2007, **129**, 8845–8849.
16 C. Y. Lai, B. G. Trewyn, D. M. Jeftinija, K. Jeftinija, S. Xu, S. Jeftinija and V. S. Lin, *J. Am. Chem. Soc.*, 2003, **125**, 4451–4459.
17 T. H. Chung, S. H. Wu, M. Yao, C. W. Lu, Y. S. Lin, Y. Hung, C. Y. Mou, Y. C. Chen and D. M. Huang, *Biomaterials*, 2007, **28**, 2959–2966.
18 C. W. Lu, Y. Hung, J. K. Hsiao, M. Yao, T. H. Chung, Y. S. Lin, S. H. Wu, S. C. Hsu, H. M. Liu, C. Y. Mou, C. S. Yang, D. M. Huang and Y. C. Chen, *Nano Lett.*, 2007, **7**, 149–154.
19 D. M. Huang, Y. Hung, B. S. Ko, S. C. Hsu, W. H. Chen, C. L. Chien, C. P. Tsai, C. T. Kuo, J. C. Kang, C. S. Yang, C. Y. Mou and Y. C. Chen, *FASEB J.*, 2005, **19**, 2014–2016.
20 S. Wang, R. Gao, F. Zhou and M. Selke, *J. Mater. Chem.*, 2004, **14**, 487–493.
21 J. Lu, M. Liong, J. I. Zink and F. Tamanoi, *Small*, 2007, **3**, 1341–1346.
22 H. Vallhov, S. Gabrielsson, M. Stromme, A. Scheynius and A. E. Garcia-Bennett, *Nano Lett.*, 2007, **7**, 3576–3582.
23 L. X. Wen, Z. Z. Li, H. K. Zou, A. Q. Liu and J. F. Chen, *Pest. Manag. Sci.*, 2005, **61**, 583–590.
24 Y. F. Zhu, J. L. Shi, Y. S. Li, H. R. Chen, W. H. Shen and X. P. Dong, *Micropor. Mesopor. Mat.*, 2005, **85**, 75–81.
25 Z. Z. Li, S. A. Xu, L. X. Wen, F. Liu, A. Q. Liu, Q. Wang, H. Y. Sun, W. Yu and J. F. Chen, *J. Control. Release*, 2006, **111**, 81–88.
26 S. Che, A. E. Garcia-Bennett, T. Yokoi, K. Sakamoto, H. Kunieda, O. Terasaki and T. Tatsumi, *Nat. Mater.*, 2003, **2**, 801–805.
27 A. E. Garcia-Bennett, K. Lund and O. Terasaki, *Angew. Chem., Int. Ed.*, 2006, **45**, 2434–2438.
28 S. Shen, A. E. Garcia-Bennett, Z. Liu, Q. Lu, Y. Shi, Y. Yan, C. Yu, W. Liu, Y. Cai, O. Terasaki and D. Zhao, *J. Am. Chem. Soc.*, 2005, **127**, 6780–6787.
29 T. Y. Ohulchanskyy, I. Roy, L. N. Goswami, Y. Chen, E. J. Bergey, R. K. Pandey, A. R. Oseroff and P. N. Prasad, *Nano Lett.*, 2007, **7**, 2835–2842.
30 P. Zhang, W. Steelant, M. Kumar and M. Scholfield, *J. Am. Chem. Soc.*, 2007, **129**, 4526–4527.
31 Y. Guo, M. Kumar and P. Zhang, *Chem. Mater.*, 2007, **19**, 6071–6072.
32 Y. Jin, S. Kannan, M. Wu and J. X. Zhao, *Chem. Res. Toxicol.*, 2007, **20**, 1126–1133.
33 C. Mehnert and J. Ying, *Chem. Commun.*, 1997, 2215–2216.
34 O.S., N. Erathodiyil, A. M. Seayad, Y. Han, S. S. Lee and J. Y. Ying, *Chem.–Eur. J.*, 2008, **14**, 3118–3125.
35 W. L. Rumsey, J. M. Vanderkooi and D. F. Wilson, *Science*, 1988, **241**, 1649–1651.
36 S. A. Vinogradov and D. F. Wilson, *Biophys. J.*, 1994, **67**, 2048–2059.
37 L. W. Lo, C. J. Koch and D. F. Wilson, *Anal. Biochem.*, 1996, **236**, 153–160.
38 R. P. Brinas, T. Troxler, R. M. Hochstrasser and S. A. Vinogradov, *J. Am. Chem. Soc.*, 2005, **127**, 11851–11862.
39 T. K. Stepinac, S. R. Chamot, E. Rungger-Brandle, P. Ferrez, J. L. Munoz, H. van den Bergh, C. E. Riva, C. J. Pournaras and G. A. Wagnieres, *Invest. Ophthalmol. Vis. Sci.*, 2005, **46**, 956–966.
40 Z. Tao, J. Goodisman and A. K. Souid, *J. Phys. Chem. A*, 2008, **112**, 1511–1518.
41 T. J. Dougherty, *Photochem. Photobiol.*, 1987, **45**, 879–889.
42 T. S. Mang, T. J. Dougherty, W. R. Potter, D. G. Boyle, S. Somer and J. Moan, *Photochem. Photobiol.*, 1987, **45**, 501–506.
43 B. W. Henderson and T. J. Dougherty, *Photochem. Photobiol.*, 1992, **55**, 145–157.
44 T. J. Dougherty, *Photochem. Photobiol.*, 1993, **58**, 895–900.
45 I. Roy, T. Y. Ohulchanskyy, H. E. Pudavar, E. J. Bergey, A. R. Oseroff, J. Morgan, T. J. Dougherty and P. N. Prasad, *J. Am. Chem. Soc.*, 2003, **125**, 7860–7865.
46 C. Kawamoto, K. Ido, T. Terada, M. Horiguchi, K. Kimura and K. Manaka, *Nippon Shokakibyo Gakkai Zasshi*, 1985, **82**, 261–269.
47 D. R. Doiron and G. S. Keller, *Curr. Probl. Dermatol.*, 1986, **15**, 85–93.
48 J. Moan, *Cancer Lett.*, 1986, **33**, 45–53.
49 I. Jin, M. Yuji, N. Yoshinori, K. Makoto and M. Mikio, *Arch. Dermatol. Res.*, 2008, **300**, 161–166.
50 S. Kim, T. Y. Ohulchanskyy, H. E. Pudavar, R. K. Pandey and P. N. Prasad, *J. Am. Chem. Soc.*, 2007, **129**, 2669–2675.
51 Y. S. Lin, C. P. Tsai, H. Y. Huang, C. T. Kuo, Y. Hung, D. M. Huang, Y. C. Chen and C. Y. Mou, *Chem. Mater.*, 2005, **17**, 4570–4573.
52 D. B. Tada, L. L. Vono, E. L. Duarte, R. Itri, P. K. Kiyohara, M. S. Baptista and L. M. Rossi, *Langmuir*, 2007, **23**, 8194–8199.
53 B. L. Frey and R. M. Corn, *Anal. Chem.*, 1996, **68**, 3187–3193.
54 R. Bonnett, *Chemical Aspects of Photodynamic Therapy*, Gordon and Breach Science Publishers, The Netherlands, 2000.
55 A. A. Krasnovskii, Jr., *Biofizika*, 1979, **24**, 747–748.